Biophysical Journal, Volume *114*

Supplemental Information

Mechanosensitivity of Cancer Cells in Contact with Soft Substrates Using AFM

Yara Abidine, Andrei Constantinescu, Valérie M. Laurent, Vinoth Sundar Rajan, Richard Michel, Valentin Laplaud, Alain Duperray, and Claude Verdier

Supporting Material

Appendix A: Numerical simulations of indentation with a three–layer model

The corrected Hertz formula for the apparent elastic modulus obtained by the indentation of a three–layer substrate proposed in Eq. 2 was assessed using the numerical model for indentation of a multilayered substrate (1). The computations are based on (i) the Papkovich-Neuber potential description of the displacements field in each layer, (ii) displacement and traction continuity across the interfaces and (iii) a frictionless contact condition using the exact shape of a rigid indenter. However several algorithmic details have been adapted to the precise shape of the AFM indenter, i.e. a rounded cone with a sharp angle of 20 degrees. The sharp angle imposed a novel estimation of the apparent contact modulus based on the geometry of the rounded cone, i.e. combining the spherical shape with a vertically shifted cone, whereas in (2, 1) only the cone was used. Moreover the starting point and the algorithm for the computation of the contact area have also been modified to insure a fast and robust convergence.

A typical example of indentation of a three–layer substrate using the AFM tip with elastic moduli and layer thicknesses of the discussed experiment is displayed in Fig. S1. The picture displays several characteristic features of the indentation of a layered medium and is coherent with experimental observations and theoretical expectations. One can remark that values of the apparent contact modulus at small indentation depth converge to the value of the apparent contact modulus of the first layer. Note that the apparent contact modulus of a material also depends on the Poisson coefficient and is not equal to the Young modulus of the material. This convergence to the apparent contact modulus was obtained after corrections based on the exact shape of the AFM indenter as explained before.

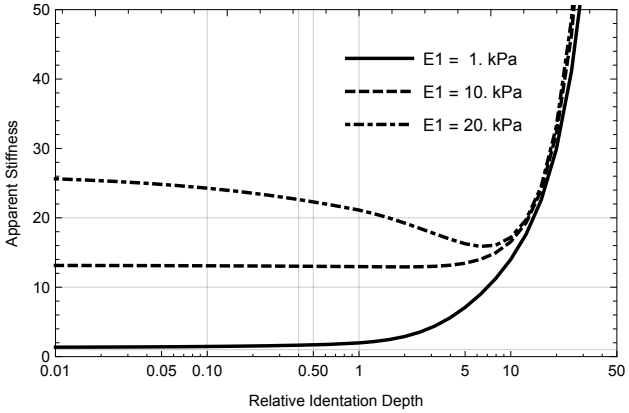

Figure S1: LogNormal plot of the apparent contact modulus $\bar{E}$ vs. reduced indentation depth δ/h_{12} for different moduli of the first layer E_1 =1, 10, 20 kPa (cell) and a second layer of E_2 =8 kPa (gel) on a very rigid substrate E_3 =70 MPa (glass). $h_1 = 10\,\mu$m and $h_2 = 70\,\mu$m. Note the minimum of the curve when $E_1 > E_2$.

Furthermore, the model predicts the apparent contact modulus of the first layer correctly even when the second layer is softer. In addition, the apparent contact modulus presents in this case a minimum located in the second layer zone as expected.

Let us further present the approximation of the correction of the Hertz formula for a three–layer system. One can first consider the apparent contact modulus $\bar{E_{12}}$ of the double layer (made of layers 1 and 2), which can be decomposed as in (2):

$$\bar{E_{12(\delta)}} = \bar{E_2} + \frac{\bar{E_1} - \bar{E_2}}{1 + (\frac{\delta}{\beta_0 h_1})^{\eta_0}} \tag{S1}$$

where $\bar{E_1} = \frac{E_1}{1-\nu_1^2}$, $\bar{E_2} = \frac{E_2}{1-\nu_2^2}$ and β_0, η_0 are adjusting constants. Constructing a similar formula, by adding the substrate (layer 3), leads to the final representation of the apparent modulus $\bar{E}_{(\delta)}$:

$$\bar{E}_{(\delta)} = \bar{E_3} + \frac{\bar{E_{12}} - \bar{E_3}}{1 + (\frac{\delta}{\beta_1 h_{12}})^{\eta_1}} \tag{S2}$$

where $\bar{E_3} = \frac{E_3}{1-\nu_3^2}$ is the apparent modulus of the substrate, $h_{12} = h_1 + h_2$ is the combined height of the two layers and β_1 and η_1 are adjusting parameters. Combining Eq. S1 and Eq. S2, one obtains using simple algebra:

$$\bar{E}_{(\delta)} = \bar{E_3} + \frac{\bar{E_2} + \frac{\bar{E_1} - \bar{E_2}}{1 + (\frac{\delta}{\beta_0 h_1})^{\eta_0}} - \bar{E_3}}{1 + (\frac{\delta}{\beta_1 h_{12}})^{\eta_1}} \tag{S3}$$

The adjusting parameters, i.e. β_0, η_0, β_1 and η_1, are obtained by fitting the apparent contact modulus in Eq. S3 with the numerical results using a least square method. Two typical adjustments are displayed in Fig. S2 *A* and *B*.

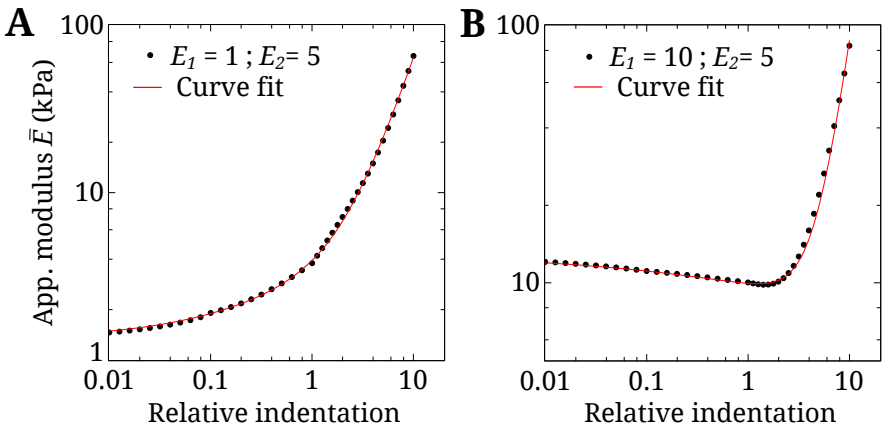

Figure S2: Comparison of the apparent contact modulus $\bar{E}_{(\delta)}$ obtained from the three–layer model *(points)* and Eq. S3 *(line)*. *(A)* $E_1 = 1$ kPa, $E_2 = 5$ kPa (and $E_3 = 70$ MPa). The fitted parameters for this curve are β_0 = 3.7, η_0 = 0.6, β_1 = 5.9 and η_1 = 1.8. *(B)* $E_1 = 5$ kPa, $E_2 = 10$ kPa (and $E_3 = 70$ MPa). The fitted parameters for this curve are β_0 = 1.55 , η_0 = 0.38, β_1 = 109 and η_1 = 2.88.

The four fitting parameters β_0, η_0, β_1 and η_1 are obtained and plotted against E_1. Fits are made, to be used in the iteration procedure, as explained in Appendix B below.

Appendix B: Linearization of the modified Hertz model of indentation

Once analytical relations for $\bar{E}(\delta)$ have been found, a linearization can be done. The indentation force F_0 applied to our sample, as a function of the indentation δ_0, is:

$$F_0 = \frac{3}{4}\,\bar{E}_{(\delta_0)}\tan\theta\;\delta_0^2 \tag{S4}$$

where θ is the pyramid half–angle. A small oscillatory amplitude δ is superposed to the indentation δ_0. Eq. S4 becomes:

$$F_0 + F = \frac{3}{4}\,\bar{E}_{(\delta_0+\delta)}\;\tan\theta\,(\delta_0+\delta)^2 \tag{S5}$$

Only terms of the first order are kept, therefore:

$$\frac{F}{\delta} = \frac{3}{2}\;\tan\theta\,\delta_0[\bar{E}_{(\delta_0)} + \frac{\delta_0}{2}\bar{E}'_{(\delta_0)}] \tag{S6}$$

Let us now differentiate the apparent modulus $\bar{E}(\delta)$ with respect to the indentation δ, from Eq. S3:

$$\begin{aligned}\bar{E}'_{(\delta)} = \frac{d\bar{E}}{d\delta} = \frac{1}{[1+(\frac{\delta}{\beta_1 h_{12}})^{\eta_1}]^2}\times \\ \frac{1}{\delta}\left[(\bar{E}_2-\bar{E}_1)\,\eta_0(\frac{\delta}{\beta_0 h_1})^{\eta_0}\,\frac{1+(\frac{\delta}{\beta_1 h_{12}})^{\eta_1}}{(1+(\frac{\delta}{\beta_0 h_1})^{\eta_0})^2}\;+\;\eta_1(\frac{\delta}{\beta_1 h_{12}})^{\eta_1}(\bar{E}_3-\bar{E}_2-\frac{\bar{E}_1-\bar{E}_2}{1+(\frac{\delta}{\beta_0 h_1})^{\eta_0}})\right]\end{aligned} \tag{S7}$$

Introducing the following variables $\chi_0 = \frac{\delta_0}{\beta_0\,h_1}$ and $\chi_1 = \frac{\delta_0}{\beta_1\,h_{12}}$, the apparent modulus in Eq. S3 is evaluated at δ_0:

$$\bar{E}_{(\delta_0)} = \frac{\bar{E}_1 + \bar{E}_2\,\chi_0^{\eta_0} + \bar{E}_3(1+\chi_0^{\eta_0})\chi_1^{\eta_1}}{(1+\chi_0^{\eta_0})(1+\chi_1^{\eta_1})} \tag{S8}$$

and $\bar{E}'_{(\delta)}$ from Eq. S7 is evaluated at $\delta = \delta_0$:

$$\begin{aligned}\bar{E}'_{(\delta_0)} = \frac{d\bar{E}}{d\delta}_{(\delta_0)} = \frac{1}{[1+\chi_1^{\eta_1}]^2}\,\frac{1}{\delta_0}\times \\ (-\bar{E}_1\left[\eta_0\,\chi_0^{\eta_0}\frac{1+\chi_1^{\eta_1}}{(1+\chi_0^{\eta_0})^2}+\eta_1\,\chi_1^{\eta_1}\,\frac{1}{1+\chi_0^{\eta_0}}\right]\;+\;\bar{E}_2\left[\eta_0\,\chi_0^{\eta_0}\frac{1+\chi_1^{\eta_1}}{(1+\chi_0^{\eta_0})^2}-\eta_1\,\chi_1^{\eta_1}\,\frac{\chi_0^{\eta_0}}{1+\chi_0^{\eta_0}}\right]\;+\;\bar{E}_3\,[\eta_1\,\chi_1^{\eta_1}])\end{aligned} \tag{S9}$$

Now let us replace the apparent modulus $\bar{E}(\delta_0)$ and $\bar{E}'(\delta_0)$ from Eq. S8–S9 into Eq. S6. We obtain:

$$\frac{F}{\delta}\,\frac{2}{3\,\tan\theta\,\delta_0} \;=\; \bar{E}_1\,k_1(\chi_0,\chi_1) + \bar{E}_2\,k_2(\chi_0,\chi_1) + \bar{E}_3\,k_3(\chi_1) \tag{S10}$$

where we have defined:

$$\begin{cases} k_1(\chi_0,\chi_1) = \dfrac{2\,(1+\chi_0^{\eta_0})(1+\chi_1^{\eta_1}) \,-\eta_0\chi_0^{\eta_0}(1+\chi_1^{\eta_1})+\eta_1\chi_1^{\eta_1}(1+\chi_0^{\eta_0})}{2(1+\chi_0^{\eta_0})^2(1+\chi_1^{\eta_1})^2} \\ k_2(\chi_0,\chi_1) = \dfrac{2\,\chi_0^{\eta_0}\,(1+\chi_0^{\eta_0})(1+\chi_1^{\eta_1})+\eta_0\chi_0^{\eta_0}(1+\chi_1^{\eta_1})-\eta_1\,\chi_1^{\eta_1}\chi_0^{\eta_0}(1+\chi_0^{\eta_0})}{2(1+\chi_0^{\eta_0})^2(1+\chi_1^{\eta_1})^2} \\ k_3(\chi_1) = \dfrac{\chi_1^{\eta_1}\,(2+\eta_1+2\chi_1^{\eta_1})}{2\,(1+\chi_1^{\eta_1})^2} \end{cases} \tag{S11}$$

It is now possible to obtain the apparent moduli $\bar{E_1}$ from Eq. S10:

$$\bar{E_1} = \frac{F}{\delta}\,\frac{2}{3\,k_1\,\tan\theta\,\delta_0} \,-\bar{E_2}\frac{k_2}{k_1} - \bar{E_3}\frac{k_3}{k_1} \tag{S12}$$

Using $E_1 = 2\,G_1\,(1+\nu_1)$, and the expressions of $\bar{E_1}$, $\bar{E_2}$ and $\bar{E_3}$, Eq. S12 can be rewritten:

$$G_1 = \frac{F}{\delta}\,\frac{1-\nu_1}{3\,\tan\theta\,\delta_0}\,\frac{1}{k_1} - E_2\frac{k_2}{k_1}\,\frac{1-\nu_1}{2(1-\nu_2^2)} - E_3\frac{k_3}{k_1}\,\frac{1-\nu_1}{2(1-\nu_3^2)} \tag{S13}$$

Let us introduce the complex force $F^*(\omega)$ and indentation $\delta^*(\omega)$; the complex shear modulus $G^*(\omega)$ of the first layer is:

$$G^*(\omega) = G_1^*(\omega) = \frac{F^*(\omega)}{\delta^*(\omega)}\,\frac{1-\nu_1}{3\,\tan\theta\,\delta_0}\,\frac{1}{k_1} - E_2^*\frac{k_2}{k_1}\,\frac{1-\nu_1}{2(1-\nu_2^2)} - E_3^*\,\frac{k_3}{k_1}\,\frac{1-\nu_1}{2(1-\nu_3^2)} \tag{S14}$$

where E_2^* and E_3^* can also be complex. When using elastic gels, we use $E_2^* = E_2$ which is real. When using endothelial cells, E_2^* is complex and was measured separately. Finally $E_3^* = E_3$ is real for the glass substrate. Eq. S14 is used to determine $G^*(\omega)$ based on an iterative process. This requires to initiate with a given value of G_1^* (close to previous ones), determine k_1, and plug it into the right hand side of Eq. S14 to find the new $G^* = G_1^*$. A few iterations (around twenty usually) are necessary to converge to the desired value $G^*(\omega)$.

Appendix C: Influence of substrate rheology and thickness

Simulations were carried out to characterize the influence of the substrate rheology and height in the three-layer model described in our study. Here we considered an apparent shear complex modulus $G_1^*(\omega)$ for the first layer (G_1^* = G_{cell}^*), and calculated the corrected modulus $G_{cor}^*(\omega)$ depending on different parameters of the substrate.

As an example, $G_1^*(\omega)$ is generated using the simplified fitting model described in Eqs. 6–7, with the following values of the parameters: G_N^0 = 2000 Pa, n_f = 0.1, k_0 = 200 Pa, g_1 = 5, a = 1.2, b = 1.5, consistent with classical cell data. Thus, the value of the modulus $|G_1^*|$[1] at low frequencies is $|G_1^*(1Hz)| \sim 2$ kPa and $E_1 \sim 3\,|G_1^*(1Hz)| \sim 6$ kPa.

The three different gels used in our study (E_2 = 5, 8, 28 kPa) were considered. Then an elastic substrate as well as a viscoelastic substrate were simulated. Finally, the sensibility to the height of the substrate was studied using three different

[1]The modulus of the complex shear modulus G* is $|G^*| = (G'^2 + G''^2)^{1/2}$

values h_2 = 2, 8, 70 µm. In all these cases, the height h_1 = 1 µm of the first layer (the cell) and the indentation δ = 400 nm of the tip were kept constant.

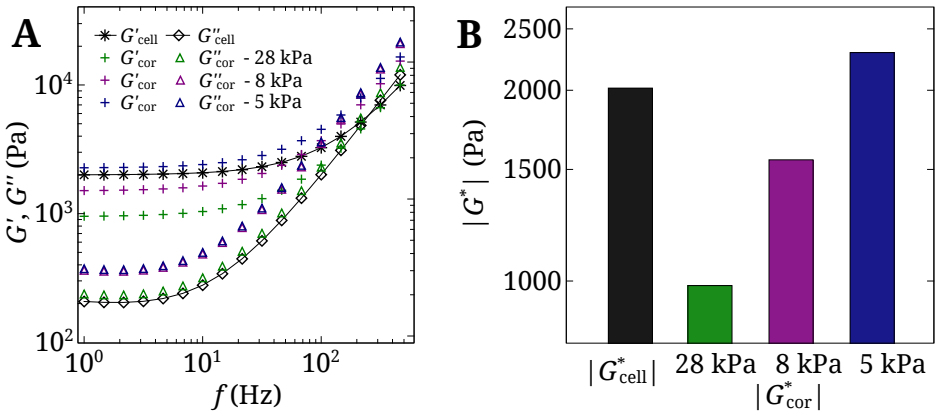

Figure S3: Substrate correction when the substrate has an elastic modulus E_2 higher, close to or smaller than the elastic modulus E_1 = 6 kPa of the first layer (cell). *(A)* Generated viscoelastic moduli of the cell $G_1^* = G_{cell}^*$ (black), and corrected viscoelastic moduli considering three values of E_2 = 5, 8, 28 kPa. *(B)* $|G_{cell}^*|$ and the corresponding values of $|G_{cor}^*|$ calculated at 1 Hz. In this simulation, h_2 = 70 µm, h_1 = 1 µm, and δ = 400 nm.

Influence of the substrate elasticity

Fig. S3 shows the influence of the second layer elastic modulus E_2 on the viscoelastic properties of the first layer ($G_1^* = G_{cell}^*$). The results can be summarized as follows, using $E_{cell} = 3\,|G_{cell}^*|$:

- If $E_{cell} > E_2$, the cell rigidity is underestimated because of the presence of a softer substrate below. Thus the correction increases the values of G' and G'' (Fig. S3 *A*, blue symbols).

- If $E_{cell} < E_2$, the cell rigidity is overestimated because of the presence of a more rigid substrate below, and the correction lowers the values of G' (Fig. S3 *A*, purple and green symbols). On the other hand, the effect on G'' depends non linearly on E_2.

The higher E_2, the higher the correction (see larger correction of E_2 = 28 kPa as compared to E_2 = 5 and 8 kPa). These results are summarized in Fig. S3 *B* where the shear modulus $|G_{cor}^*|$ at 1 Hz is represented in the three cases.

Comparison between an elastic substrate and a viscoelastic substrate

When we considered a viscoelastic substrate with high values of G'' (like the layer of HUVECs, Fig. S4 *A*), the cell viscous component was affected as follows:

- If $G''_{cell} > G''_{substrate}$, the cell viscous component is underestimated, and the correction increases G''_{cell}.

- If $G''_{cell} < G''_{substrate}$, the cell viscous component is overestimated, and the correction decreases G''_{cell} as shown in Fig. S4 *B* (turquoise).

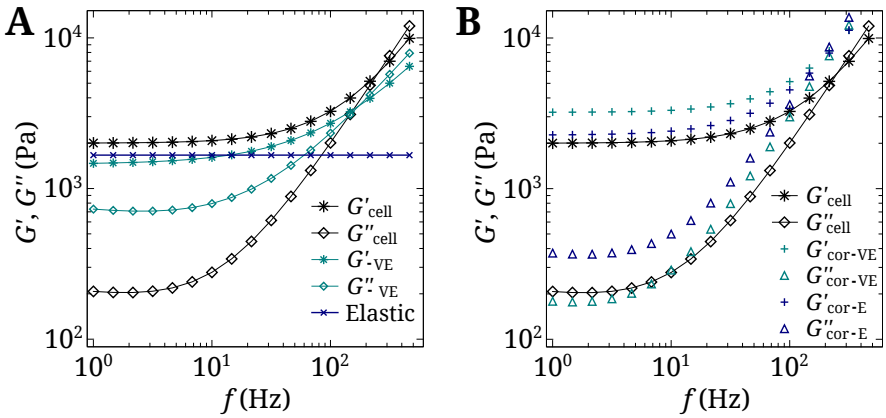

Figure S4: Correction of the apparent modulus G^*_{cell} considering an elastic substrate and a viscoelastic one. *(A)* Apparent viscoelastic moduli of the cell G^*_{cell} (black), of the substrate G^*_{VE} (turquoise) with $|G^*_2(1Hz)|$ = 1.7 kPa, and corresponding elastic substrate $E_2 = 5\text{kPa} \sim 3\,|G^*_2(1Hz)|$ kPa (blue). The viscoelastic moduli of the substrate were generated using the fitting model. *(B)* Corrected viscoelastic moduli considering the viscoelastic substrate (turquoise) and the elastic substrate (blue).

Considering only an equivalent elastic substrate (same $|G^*_2(1Hz)|$ = 1.7 kPa, $E_2 \sim 5$ kPa) gave rise to different G' and G'' (blue). Therefore the precise contribution of the viscoelasticity of the substrate is important as it affects both G' and G''.

Influence of substrate height – Justification of the HUVEC thin layer model

Fig. S5 shows the effect of substrate height h_2 when cells are in contact with an 8 kPa thin layer. In this case, the high value of E_2 leads to overestimation of the moduli G' and G'', so a diminution of h_2 increases substrate effects, lowering G' and G''. But the correction is very small.

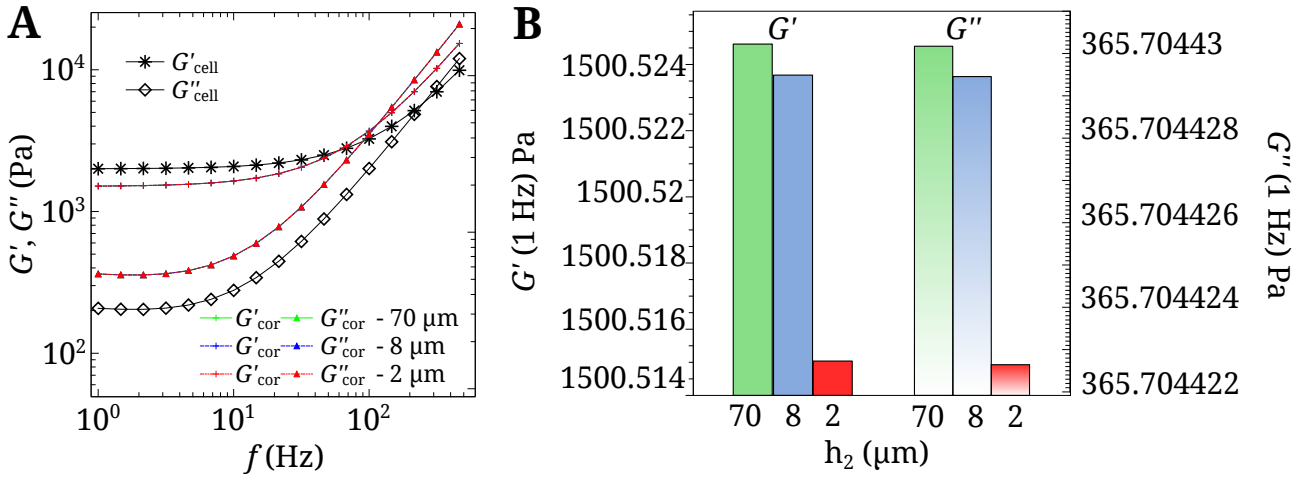

Figure S5: Correction of the apparent modulus G^*_{cell} considering three different substrate heights h_2 = 2, 8, 70 µm. The other parameters are: E_2 = 8 kPa, h_1 = 1 µm and δ = 0.4 µm.

This is due to the fact that the relative indentation depth $\frac{\delta}{h_{12}}$ is always very small in this case. Indeed, as shown in Fig. S1, the apparent stiffness remains almost constant for small relative indentation depths (lower than 0.1), which is the case in most experiments involving the HUVEC monolayer simulated here. The correction mainly comes here from the elasticity E_2 of the underlying substrate (E_2 = 8 kPa), as already seen in Fig. S3 *B*, but the thickness is not so important. This is a justification of our approach of the endothelial layer, which can be mimicked by a thin layer, even though it has a waviness corresponding to hollows and bumps (thickness between 2 and 8 μm). Therefore we can assume that the substrate height does not influence much the corrected values of the viscoelastic moduli.

Appendix D: Cancer cell transmigration through the endothelium

Movie S1 provides adequate evidence of the cancer cell passage through the endothelium.

Transmigration of cancer cell. A J82 cancer cell is tagged with Actin–GFP (green) and endothelial cells (purple) are stained using CellTrace Far Red DDAO-SE from Life technologies. Beads also appear in red and indicate the gel (8 kPa) upper surface. At the beginning of transmigration, the endothelial cells are seen from below showing no trace of tumor cell. Then a view from the side shows the dynamic process followed by the cancer cell, penetrating through the endothelial monolayer. At the end, a view from below shows the cancer cell (green) after eventually passing through the endothelium.

Supporting references

1. Constantinescu, A., A. Korsunsky, O. Pison, and A. Oueslati, 2013. Symbolic and numerical solution of the axisymmetric indentation problem for a multilayered elastic coating. *Int. J. Solids Struct.* 50:2798–2807.

2. Korsunsky, A. M., and A. Constantinescu, 2009. The influence of indenter bluntness on the apparent contact stiffness of thin coatings. *Thin Solid Films* 517:4835–4844.